Reduced-Order Modelling Method of Grid- Connected Inverter With Long Transmission Cable

Zhou, Weihua; Wang, Yanbo; Chen, Zhe

Reduced-Order Modelling Method of Grid-Connected Inverter With Long Transmission Cable

Weihua Zhou[*], Yanbo Wang[†], and Zhe Chen[‡]
Department of Energy Technology
Aalborg University
Aalborg, Denmark
[*]wez@et.aau.dk, [†]ywa@et.aau.dk, [‡]zch@et.aau.dk

Abstract—This paper presents a reduced-order modelling method for grid-connected inverter (GCI) with long transmission cable (LTC). State-space models of GCI and LTC are first obtained from frequency characteristics of terminal impedance by applying vector fitting (VF) algorithm rather than conventional mathematical modelling. Then, Prony analysis (PA) and balanced truncation (BT) algorithms are employed to find an optimized order number of state-space model. Finally, a reduced-order model of GCI with LTC is established by removing non-dominant poles of original state-space model. Simulation results show that the proposed reduced-order modelling method is able to accurately obtain dominated poles of system, and reveal practical terminal impedance characteristics. The proposed method may simplify modelling procedure and improve computational efficiency for small signal stability analysis.

Index Terms—Grid-connected inverter, long transmission cable, reduced-order modelling, small-signal stability, vector fitting.

I. Introduction

The increasing penetrations of renewable energy sources, such as wind power plants and photovoltaic power plants, are arising to new emerging challenges. Stability issue is one of concerns. Various instability issues have been intensively reported in [1]–[3]. Low-frequency oscillation may be induced due to interaction of synchronous control loop with time-varying grid impedance [3]. Also, sub-synchronous oscillation phenomena have been concerned in [4], which may be caused due to coupling of controllers between grid-connected inverters (GCIs) and series compensation or FACTS (flexible alternative current transmission system) devices. In addition, the harmonic-frequency oscillation has been frequently reported in [5], [6], which may be generated due to the interactions between inner current control loop and passive components of GCIs. These oscillation phenomena are challenging the safe operation of power system.

Apart from aforementioned factors associated with control system of GCI, several potential factors in transmission system such as distributed parasitic capacitors of long transmission cable (LTC) may also result in oscillation phenomenon [7]. Thus, several modelling and analysis methods have been developed to predict small-signal instability resulting from LTC [6]–[13]. In detail, the cascaded-Π circuit models of LTC are built in [6]–[13]. However, practical frequency-dependent characteristics of LTC is not revealed in [6], [8]–[11], which fails to perform effective stability analysis due to the lack of corresponding damping characteristics. To reveal practical frequency characteristics and corresponding damping characteristics of LTC, an improved cascaded-Π circuit model is developed in [12], [13], where a series of extra RL branches are paralleled with each Π section of conventional cascaded-Π circuit. However, it's difficult to obtain parameters of the extra RL branches accurately. Also, the presence of RL branches causes a high-order state-space model, which thus is not easy to perform stability assessment due to complicated modelling procedure and high computational burdens.

State space-based method is a well-established small-signal stability analysis tool, which can determine participation factor of different state variables on oscillation modes, and reveal origins of resonance phenomena [5], [12], [13]. System model is first linearized at a certain operation point, and state matrix of the linearized model is calculated. Then, stability can be evaluated by identifying the eigenvalues distribution of the state matrix in complex plane [5], [12], [13]. However, the full-order state-space model of GCI with LTC is not applicable because of the high order of LTC [13].

Therefore, this paper presents a reduced-order modelling method for GCI with LTC. Reduced-order state-space model of GCI is directly obtained from frequency characteristics of terminal impedance by applying vector fitting (VF) algorithm instead of mathematical modelling. Similarly, state-space model of LTC is also fitted by VF algorithm. Also, Prony analysis (PA) and balanced truncation (BT) algorithms are employed to calculate optimized order number of the state-space model. Then, the reduced-order model can be formulated by removing non-dominant poles of the original state-space model.

The main contributions of this paper are briefly explained as follows. (1) Reduced-order modelling procedure of GCI with LTC is established on the basis of PA, VF and BT; (2) The frequency and damping characteristics of LTC is revealed by the proposed reduced-order modelling method. (3) State-space model is established by fitting frequency characteristics

Fig. 1. Three-phase GCI connected with LTC.

Fig. 2. Block diagram of single current control loop in dq domain.
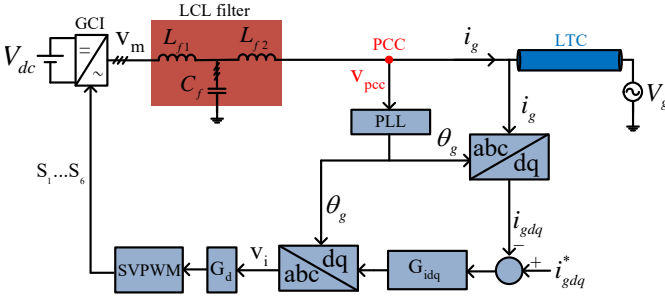
of terminal impedance without using mathematical derivation.

The rest of this paper is organized as follows. System description and frequency characteristics of terminal impedances for both GCI and LTC are depicted in Section II. Section III introduces the mathematical basis of PA, VF and BT, and explanation of the proposed reduced-order modelling method for both GCI and LTC is also given. The detailed implementation of the proposed method is shown in Section IV. Simulation results are given in Section V to validate the reduced-order model. Conclusions are drawn in Section VI .

II. SYSTEM DESCRIPTION AND TERMINAL IMPEDANCE CHARACTERISTICS OF GCI AND LTC

To explain the proposed reduced-order state-space modelling method, the exemplified power system is first explained and frequency characteristics of terminal impedances of GCI and LTC are then derived in this section.

A. System description

Fig. 1 shows a three-phase GCI system connected with LTC. The dc-link voltage V_{dc} is considered as constant. Besides, a LCL filter is applied to decrease the switching harmonic of grid current. A synchronous reference frame phase-locked loop (SRF-PLL) detects the instant frequency and angle of grid voltage to synchronize the GCI and grid. Single current loop control in dq-domain with PI controller G_{idq} is used.

B. Terminal impedance characteristics of GCI and LTC

To establish a reduced-order model of grid-connected inverter with LTC using the proposed method, their terminal impedance characteristics are derived in this section.

1) Terminal impedance characteristics of GCI: It should be noted that this paper focuses on extracting out the state-space model from a set of terminal impedance responses using VF, instead of accurately measuring output impedance of the GCI, since already many papers were about the topic [14], [15]. Besides, the terminal characteristics sometimes can be obtained from the manufacturers. So in the proposed reduced-order state-space modelling method, the terminal frequency response of GCI is obtained directly from the theoretically derived value.

To derive the theoretical terminal impedance characteristics of GCI Z_{inv}, block diagram of GCI part is depicted in Fig. 2. G_d is the digital delay, and includes two parts: one sampling
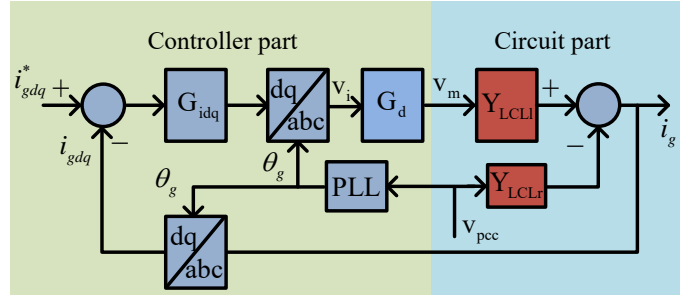
period delay for computation, half sampling period delay for PWM modulation. Y_{LCLl} and Y_{LCLr} are defined using the basic circuit principal,

$$G_{idq} = K_p + \frac{K_i}{s} \tag{1}$$

$$G_d = e^{-1.5T_s s} \tag{2}$$

$$Y_{LCLl} = \left. \frac{i_g}{v_m} \right|_{v_{pcc}=0} = \frac{\frac{1}{sC_f}}{(\frac{1}{sC_f}//sL_{f2} + sL_{f1})(\frac{1}{sC_f} + sL_{f2})} \tag{3}$$

$$Y_{LCLr} = \left. \frac{i_g}{v_{pcc}} \right|_{v_m=0} = \frac{1}{(\frac{1}{sC_f}//sL_{f1} + sL_{f2})}$$

The impact of PLL on the output impedance of the GCI can be ignored if the bandwidth of PLL is small enough [16]. The output impedance equivalent is shown as follows, which is just like the formula for single-phase power system, simplifying the following analysis.

$$Z_{inv} = -\frac{v_{pcc}}{i_g} = \frac{1 + T_{SYS}}{Y_{LCLr}} \tag{4}$$

where T_{SYS} is the open-loop transfer function. The circuit and controller parameters are given in Table I. The analytically-derived terminal impedance characteristics of the GCI using (4) is shown as the blue line in Fig. 3.

TABLE I. SYSTEM PARAMETERS OF THE EXEMPLIFIED GRID-CONNECTED INVERTER

| Parameter	Value
dc-link voltage V_{dc}	600V
Grid fundamental frequency	50Hz
Filter inductor L_{f1}	10mH
Filter inductor L_{f2}	10mH
Filter capacitor C_f	2μF
Switching frequency f_s	10kHz
Sampling frequency f_{samp}	10kHz
Grid voltage (phase-to-phase) V_g	380V
Proportional gain of current controller K_p	0.08
Integral gain of current controller K_i	200
Proportional gain of PLL K_p	0.18
Integral gain of PLL K_i	3.2
D-axis current command i_{gd}^*	30A
Q-axis current command i_{gq}^*	0
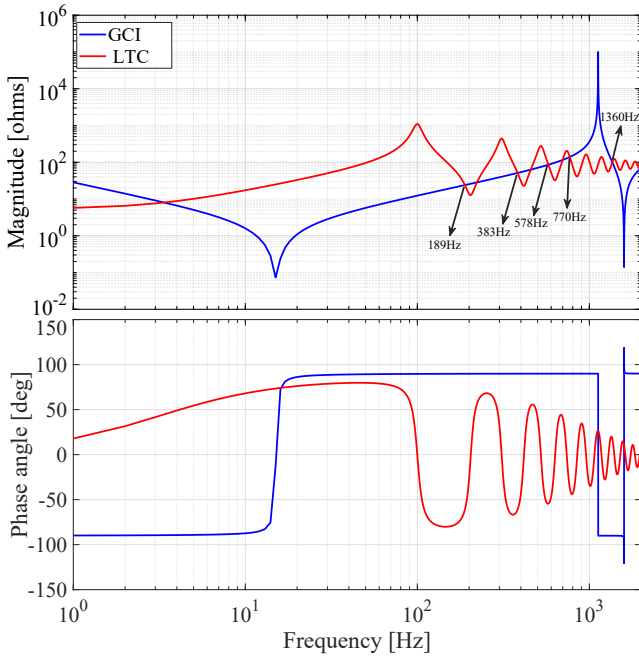
Fig. 3. Terminal impedance frequency characteristics of GCI and LTC.

2) Terminal impedance characteristics of LTC: Terminal impedance characteristics of LTC can be theoretically calculated, if the physical parameters are known [13]. The theoretical terminal impedance characteristics of a 100km LTC with one end short-circuit is shown as the red line in Fig.3. It can be seen that the LTC has multiple resonance peaks, among which peak magnitudes decrease when frequency increases due to the inherent damping characteristics.

III. THE PROPOSED REDUCED-ORDER MODELLING METHOD

In this section, the proposed reduced-order modelling method is introduced. In the proposed method, the reduced-order model of GCI is obtained by directly applying VF to its terminal impedance characteristics, and the reduced-order model of LTC is obtained by applying PA, VF and BT. So the principal of PA, VF and BT is first reviewed, and the implementation of the proposed method is then presented.

A. Concept and basis of VF, PA and BT

1) VF: VF is a fitting algorithm that is able to generate a system mathematical model by fitting terminal impedance characteristics [17],

$$f(s) = \sum_{n=1}^{N} \frac{R_n}{s - P_n} + D + sE \quad (5)$$

where $f(s)$ is the fitted transfer function, N is the order of the transfer function, R_n and P_n are the nth residue and pole pair. D is nonzero if the order of the numerator polynomial is not lower than the order of denominator polynomial. And E indicates the transfer function is improper [17]. To obtain above values, two-stage identification process is executed.

First, the poles are identified by iteratively changing initial starting poles which are user-defined and generally spaced evenly in the frequency range of interest. Then, the residues, D and E can be obtained based on the poles. (5) can be easily transferred into state-space representation as,

$$\begin{aligned} sx &= Ax + Bu \\ y &= Cx + (D + sE)u \end{aligned} \quad (6)$$

where x is the state variables, u is the input variable, y is the output variable, $A = diag(P_1, P_2, ...P_N)$, B is the $n \times 1$ unit vector, $C = diag(R_1, R_2, ...R_N)$. D and E are the same as in (5). The most attracting point of VF is that it can directly obtain the state-space model from the terminal impedance characteristics without internal information.

2) PA: PA fits N evenly spaced time-domain samples by several damped sinusoidal signals [18],

$$f(t) = \sum_{i=1}^{M} A_i e^{\sigma_i t} \cos(2\pi f_i t + \phi_i) \quad (t = t_0, t_2...t_{N-1}) \quad (7)$$

where A_i, σ_i, f_i, ϕ_i is the ith amplitude, damping coefficient, frequency, and phase angle, respectively. Actually, the only difference with FFT is that PA can obtain the damping coefficient of each sinusoidal component in addition to amplitude, frequency and phase angle. Based on Euler's formula, (7) is transferred into the following form,

$$f(t) = \sum_{i=1}^{M} \frac{1}{2} A_i e^{\pm j\phi_i} e^{\lambda_i t} (t = t_0, t_2...t_{N-1}) \quad (8)$$

where $\lambda_i = \sigma_i \pm j2\pi f_i$ is the ith eigenvalue. Similar to VF, PA also contains a two-stage identification process which identifies $e^{\lambda_i t}$ and $A_i e^{\pm j\phi_i}$, respectively. However, PA can determine the order of the system directly using SVD instead of a trail-and-error method in VF, which is much more time-efficient when the order is very high. So PA is used to identify the system order in the proposed three-step reduced-order modelling. In principal, the error-bonded order can be obtained by eliminating several small singular values by rearranging the N samples in the following form,

$$F = \begin{bmatrix} f(M-1) & f(M-2) & \cdots & f(0) \\ f(M) & f(M-1) & \cdots & f(1) \\ \vdots & \vdots & \ddots & \vdots \\ f(N-2) & f(N-3) & \cdots & f(N-1-M) \end{bmatrix} \quad (9)$$

where M is the user-defined order, and N is the number of the evenly spaced samples. Define the singular values of F are $s_i(F), i = 1, 2...s$. If the several largest singular values are much more dominant than the rest smaller singular values,

$$\sigma_1^2 + \sigma_2^2 + ...\sigma_k^2 \gg \sigma_{k+1}^2 + \sigma_{k+2}^2 + ...\sigma_s^2 \quad (10)$$

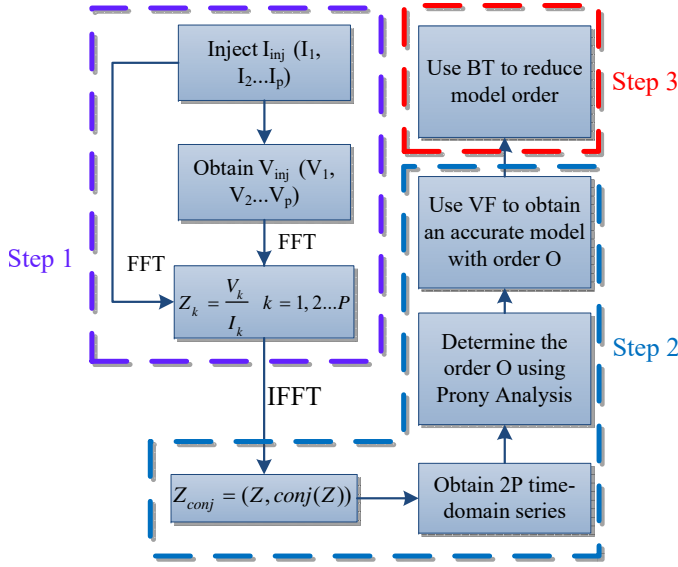the state variables with smaller singular values can be omitted directly, and k is the reduced order of the system.

Fig. 4. Procedure of the proposed reduced-order modelling approach.

Fig. 5. Vector fitting result of terminal frequency responses of GCI.

3) BT: BT algorithm consists of balance stage and truncation stage literally. For a LTI system like (6), the balance stage aims to find a similarity transformation matrix which transforms the original observability Gramian and controllability Gramian to the same diagonal matrixes, of which the diagonal elements are hankel singular values (HSVs).

The aim of truncation stage is to retain the state variables with large HSVs. If k satisfies (10), then $\sigma_{k+1}, \sigma_{k+2}...\sigma_s$ can be omitted. Actually, the dynamic performance and input-output relationship keep almost unchanged after truncation because the retained state variables are much more observable and controllable than those omitted state variables.

B. The proposed reduced-order modelling method

The procedure of the proposed reduced-order modelling approach is shown in Fig.4.

1) Step 1: Small current disturbances which include P evenly-spaced frequencies are injected at the LTC terminal,

$$I_{inj} = \sum_{k=1}^{P} A_k \cos(2\pi(f_{start} + \frac{f_{end} - f_{start}}{P}k)t) \quad (11)$$

where A_k is the magnitude of the kth current component and $A_k(k = 1, 2..., P)$ are equal. f_{start} and f_{end} are the starting frequency and the ending frequency of the frequency range of interest. Then the corresponding terminal voltage response V_{inj} can be decomposed into the sum of the P frequency components using FFT:

$$V_{inj} = \sum_{k=1}^{P} B_k \cos(2\pi(f_{start} + \frac{f_{end} - f_{start}}{P}k)t + \varphi_k) \quad (12)$$

where B_k and φ_k are the magnitude and phase angle of the kth voltage response component, respectively. So the terminal output impedance of the LTC at frequency f_k is,

$$Z(2\pi f_k) = \frac{B_k}{A_k}(\cos(\varphi_k) + i\sin(\varphi_k)) \quad (13)$$
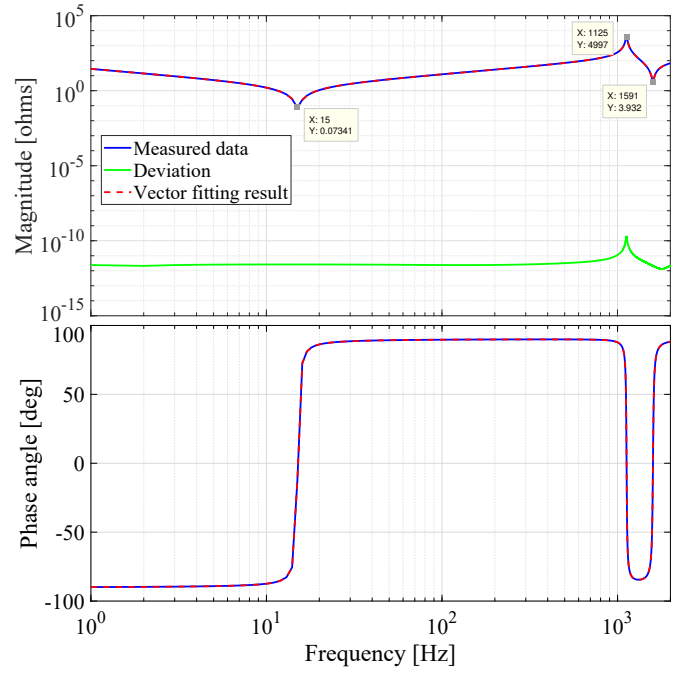
where B_k/A_k and φ_k are the amplitude and phase of the kth frequency response, which will be used to fit a transfer function or a state space representation using VF.

2) Step 2: The frequency responses obtained in step 1 are used to determine the high order which satisfies error requirement. In detail, conjugate symmetry is firstly used to add negative frequency components in the spectrum:

$$Z(2\pi f_k)_{con} = \frac{B_k}{A_k}(\cos(\varphi_k) - i\sin(\varphi_k)) \quad (14)$$

Then, IFFT transforms the $2P$ frequency-domain samples to $2P$ time-domain samples: $f(t_1), f(t_2)..., f(t_{2P})$. (9) are used to determine the high order where $M = P, N = 2P$.

3) Step 3: BT is employed to reduce the order of the high-order state-space model obtained in step 2. Final order of the reduced-order model is determined by the number of preserved peaks.

IV. REDUCED-ORDER MODELLING OF GCI AND LTC

In this section, reduced-order models for both GCI and LTC are obtained using the proposed method.

A. Reduced-order modelling of GCI

2000 evenly-spaced frequency points between 1Hz and 2kHz on the blue line in Fig. 3 are fitted by VF, and the fitting result is shown in Fig. 5. When implementing VF, system order increases gradually until the fitting error meets the requirement. It can be seen from Fig.5 that the deviation between the original data and the vector fitting result is only 10^{-10} when the system order is chosen as 5. However, the fitted 5-order model is improper since the E component in (6) is non-zero. Actually, it's the filtering inductor L_{f2} that
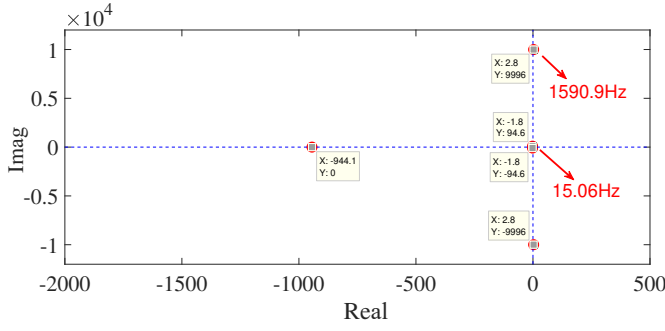
Fig. 6. Eigenvalues of 5-order GCI output admittance.

Fig. 7. Frequency responses of practical WideBand Line model and established reduced-order models.

makes the fitted model improper, and E is exactly the value of inductor L_{f2}. In this case, the admittance form of the inverter has to be adopted, which can be easily obtained from the fitted impedance equivalent formula. The fitted inverter admittance expression is shown as following,

$$sx_{inv} = A_{inv}x_{inv} + B_{inv}u \\ y = C_{inv}x_{inv} + D_{inv}u \quad (15)$$

where

$$A_{inv} = \begin{bmatrix} -942 & -12200 & -2820 & -144 & -384 \\ 8190 & 0 & 0 & 0 & 0 \\ 0 & 4100 & 0 & 0 & 0 \\ 0 & 0 & 256 & 0 & 0 \\ 0 & 0 & 0 & 256 & 0 \end{bmatrix}$$

$$B_{inv} = \begin{bmatrix} 32 & 0 & 0 & 0 & 0 \end{bmatrix}^T$$
$$C_{inv} = \begin{bmatrix} 3.13 & 0.359 & 4.66 & 17.1 & 0 \end{bmatrix}$$
$$D_{inv} = \begin{bmatrix} 0 \end{bmatrix}$$

$$(16)$$

The eigenvalues of A_{inv} are plotted in Fig.6. Because magnitude is the reciprocal of the admittance, the two local minimum frequencies 1591Hz and 15Hz of magnitude curve in Fig. 5 are exactly the two peak frequencies of admittance curve. Considering the negligible discrepancy between 1591Hz and 1590.9Hz, 15Hz and 15.06Hz, VF captures accurately the peaks, demonstrating the effectiveness of the fitting algorithm.

The full-order model of grid-connected inverter has about 15 order [19]. Therefore, the fitted 5-order model is actually a reduced-order model.

B. Reduced-order modelling of LTC

To verify the effectiveness of the proposed reduced-order modelling method, a WideBand Line model which has the same physical parameters as the above 100km LTC is adopted. The advanced frequency-dependent WideBand Line model is provide by OPAL-RT ARTEMiS-SSN library, and it can be easily integrated into Matlab/Simulink model for time-domain simulation [20]. The reduced-order model of the WideBand Line model is derived based on the three steps in Fig. 4.

1) Step 1: Current disturbances including 2000 frequency samples which are equally distributed in 1-2000Hz range are injected into the terminal of WideBand Line model. And terminal terminal characteristics are calculated by applying FFT
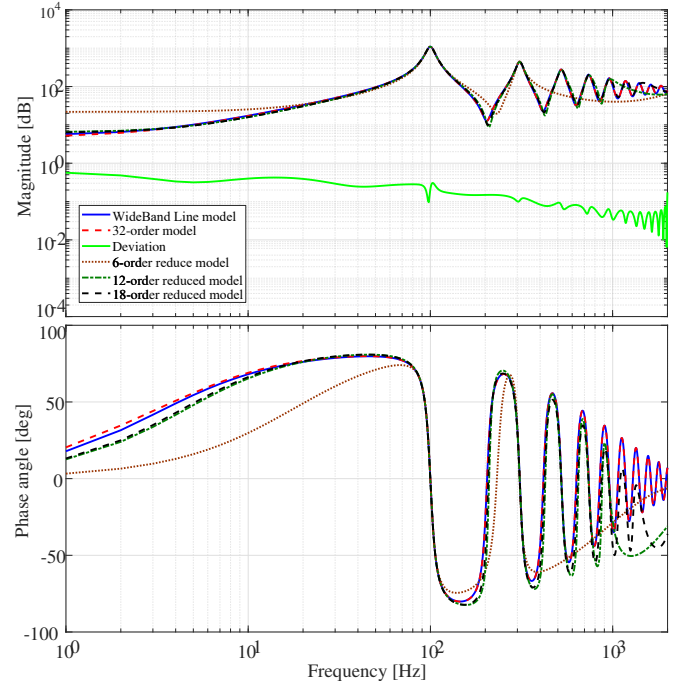
to both injected current and corresponding voltage response (shown as the blue line in Fig. 7).

2) Step 2: The conjugate symmetry forms of the 2000 frequency responses are first added to the frequency series obtained in step 1. Then, PA extracts out the high order 32 from the corresponding time-domain series which are obtained by applying IFFT to the 4000 frequency series. The frequency response of the fitted 32-order model is shown as the red dotted line in Fig. 7. Actually, the fitting error of the 32-order high-order model is 0.0994, which is small enough.

3) Step 3: Reduced-order models are obtained from the 32-order model by using BT to preserve the dominant state variables and eliminate the less dominant state variables. The frequency responses of 6-order, 12-order and 18-order reduced models are also depicted in Fig. 7.

It's clear that the number of preserved dominant resonance peaks increases as the order of the reduced model increases, thus expanding the fitted frequency range.

C. Time-Domain Dynamic Performance Comparisons

To further analyzes and compare different reduced-order models, comparative analysis of different state-space models and the original WideBand Line model under step disturbance are shown in Fig.8.

It can be seen from Fig. 8 that step responses of the 32-order model approximates original WideBand Line model very well. In addition, time-domain approximation ability of the reduced-order model increases as the order increases, which agrees with the above frequency-domain fitting results. It should be noted that the tradeoff between complexity and accuracy should be made.
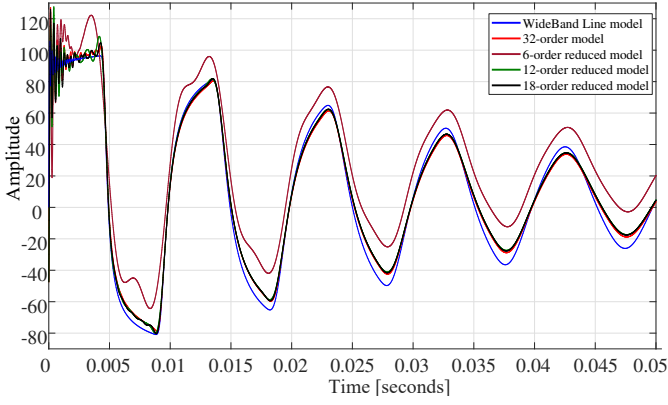
Fig. 8. Step responses of different reduced-order models and WideBand Line model.
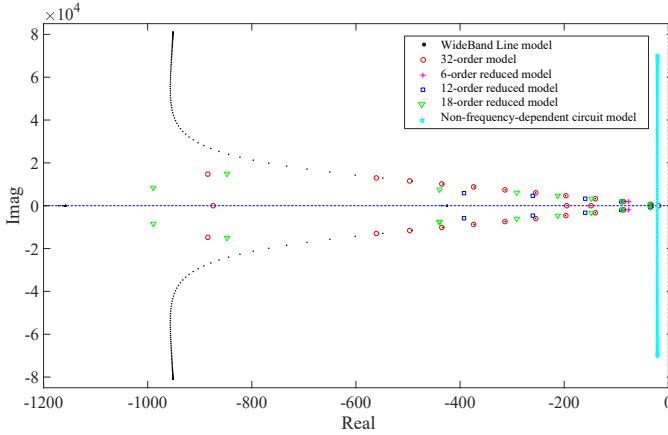

Fig. 9. Eigenvalues of WideBand Line model, reduced-order models and non-frequency-dependent circuit model.

The eigenvalues of the WideBand Line model, reduced-order models and non-frequency-dependent circuit model are shown in Fig. 9. It can be seen that the most dominant eigenvalues of WideBand Line model are captured by all 6-order, 12-order and 18-order reduced models. And the ability to capture the higher-frequency eigenvalues increases as the order increases. The 32-order model can capture all of the eigenvalues up to 2kHz. However, the non-frequency-dependent circuit model loses the damping information and cannot reflect internal modes of LTC, thus leads to inaccurate small-signal stability conclusion.

V. Simulation Verification

To verify the effectiveness of the proposed reduced-order modelling method of GCI with LTC. System eigenvalues are shown in Fig. 10, which are calculated using original WideBand Linde model, reduced models (6-order, 12-order, 18-order, 32-order) and cascaded-Π circuit without consideration of frequency dependence and corresponding damping characteristics.

It can be seen from Fig. 10 that if non-frequency-dependent LTC circuit model is adopted, inaccurate small-signal stability conclusion is obtained even the circuit model order is very
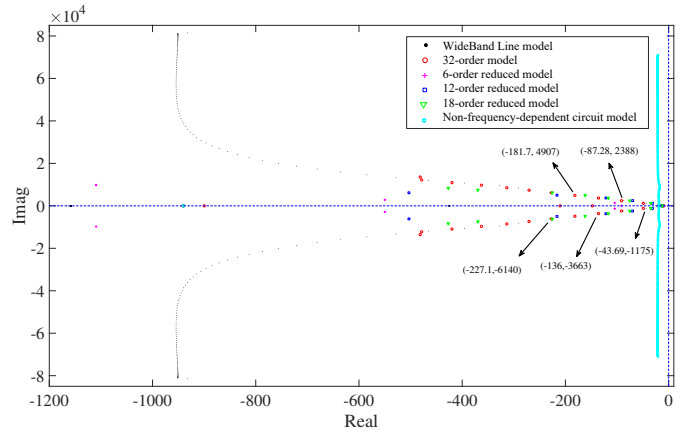

Fig. 10. System eigenvalues with different state-space models of LTC.

high, which results from the lack of representation of corresponding damping characteristics. The interaction modes can be captured by the different reduced-order models, and capture ability increases as the order of the reduced model increases, which means that low-order reduced frequency-dependent models can obtain more accurate small-signal stability conclusion than high-order model without consideration of frequency dependence and corresponding damping characteristics.

To further verify the effectiveness of the reduced-order models, time-domain simulation is performed. Grid current and its frequency spectrum are shown in Fig. 11. It's clear from Fig. 10 that all reduced-order models reveal the oscillation frequencies with damping coefficient, which is not revealed by the conventional non-frequency-dependent circuit model.

VI. Conclusion

This paper presents a reduced-order modelling method of GCI with LTC. State-space models of inverter and LTC are established by fitting terminal frequency characteristics instead of mathematical derivation. Then, PA and BT algorithms are employed to optimize the order number of state-space model. Finally, the reduced-order model of GCI with LTC is formulated by removing non-dominant poles of original state-space model. Comparative analysis of reduced-order models and WideBand Line model shows that the proposed method is able to accurately obtain dominated poles of system, and reveal practical frequency characteristics. Furthermore, Simulation results are given to validate the proposed reduced-order modelling method. The proposed method may simplify modelling procedure and improve computational efficiency for small signal stability analysis.

References

[1] Z. Chen, J. M. Guerrero, and F. Blaabjerg, "A review of the state of the art of power electronics for wind turbines," *IEEE Trans. Power Electron.*, vol. 24, no. 8, pp. 1859–1875, Aug. 2009.

[2] W. Wu, Y. Liu, Y. He, H. S.-H. Chung, M. Liserre, and F. Blaabjerg, "Damping methods for resonances caused by lcl-filter-based current-controlled grid-tied power inverters: An overview," *IEEE Trans. Ind. Electron.*, vol. 64, no. 9, pp. 7402–7413, Sept. 2017.
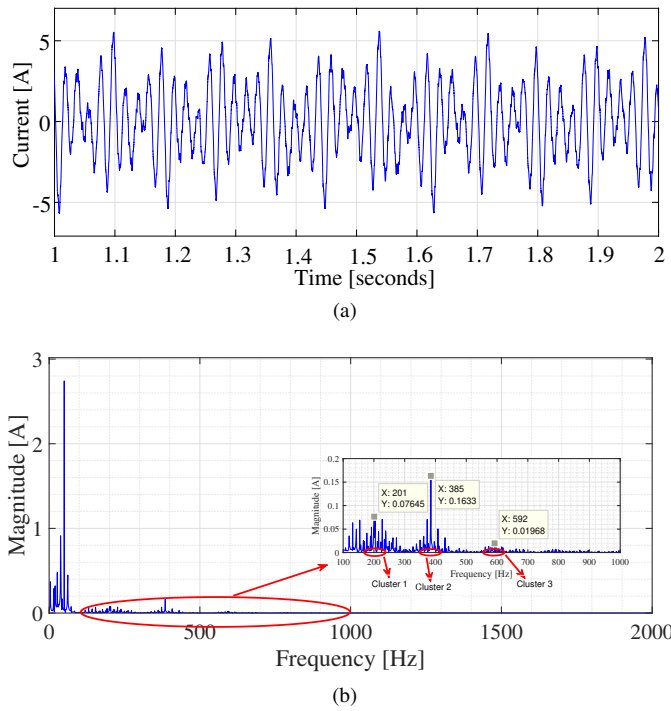
Fig. 11. Time-domain and frequency-domain waveform of grid current. (a) Time-domain waveform of grid current; (b) FFT analysis of grid current.

[3] D. Dong, B. Wen, D. Boroyevich, P. Mattavelli, and Y. Xue, "Analysis of phase-locked loop low-frequency stability in three-phase grid-connected power converters considering impedance interactions," *IEEE Trans. Ind. Electron.*, vol. 62, no. 1, pp. 310–321, Jan. 2015.

[4] H. A. Mohammadpour and E. Santi, "Modeling and control of gate-controlled series capacitor interfaced with a dfig-based wind farm," *IEEE Trans. Ind. Electron.*, vol. 62, no. 2, pp. 1022–1033, Feb. 2015.

[5] Y. Wang, X. Wang, F. Blaabjerg, and Z. Chen, "Harmonic instability assessment using state-space modeling and participation analysis in inverter-fed power systems," *IEEE Trans. Ind. Electron.*, vol. 64, no. 1, pp. 806–816, Jan. 2017.

[6] Y. Song, E. Ebrahimzadeh, and F. Blaabjerg, "Analysis of high frequency resonance in DFIG-based offshore wind farm via long transmission cable," *IEEE Trans. Energy Convers.*, Early Access.

[13] J. Beerten and S. D'Arco, "Frequency-dependent cable modelling for

[7] S. Zhang, S. Jiang, X. Lu, B. Ge, and F. Z. Peng, "Resonance issues and damping techniques for grid-connected inverters with long transmission cable," *IEEE Trans. Power Electron.*, vol. 29, no. 1, pp. 110–120, Jan. 2014.

[8] X. Wang, F. Blaabjerg, and P. C. Loh, "Proportional derivative based stabilizing control of paralleled grid converters with cables in renewable power plants," in *Proc. Energy Convers. Congr. and Expo.*, 2014, pp. 4917–4924.

[9] Y. Song, F. Blaabjerg, and X. Wang, "Analysis and active damping of multiple high frequency resonances in DFIG system," *IEEE Trans. Energy Convers.*, vol. 32, no. 1, pp. 369–381, Mar. 2017.

[10] X. Zhang, H. S.-h. Chung, L. L. Cao, J. P. W. Chow, and W. Wu, "Impedance-based stability criterion for multiple offshore inverters connected in parallel with long cables," in *Proc. Energy Convers. Congr. and Expo.* IEEE, 2017, pp. 3383–3389.

[11] H. Wang, T. Saha, and R. Zane, "Impedance-based stability analysis and design considerations for DC current distribution with long transmission cable," in *Proc. Control and Modeling for Power Electronics (COMPEL).* IEEE, 2017, pp. 1–8.

[12] J. Beerten, S. D'Arco, and J. A. Suul, "Identification and small-signal analysis of interaction modes in VSC MTDC systems," *IEEE Trans. Power Del.*, vol. 31, no. 2, pp. 888–897, April 2016.
small-signal stability analysis of VSC-HVDC systems," *IET Gen., Transm. Distrib.*, vol. 10, no. 6, pp. 1370–1381, May 2016.

[14] B. Wen, R. Burgos, D. Boroyevich, P. Mattavelli, and Z. Shen, "Ac stability analysis and dq frame impedance specifications in power-electronics-based distributed power systems," *IEEE J. Emerg. Sel. Topics Power Electron.*, vol. 5, no. 4, pp. 1455–1465, Dec. 2017.

[15] Y. Wang, X. Wang, F. Blaabjerg, and Z. Chen, "Frequency scanning-based stability analysis method for grid-connected inverter system," in *Proc. of IEEE 3rd Intern. Future Energy Electron. Conf.* IEEE, 2017, pp. 1575–1580.

[16] A. Rygg, M. Molinas, C. Zhang, and X. Cai, "On the equivalence and impact on stability of impedance modeling of power electronic converters in different domains," *IEEE J. Emerg. Sel. Topics Power Electron.*, vol. 5, no. 4, pp. 1444–1454, Dec. 2017.

[17] B. Gustavsen and A. Semlyen, "Rational approximation of frequency domain responses by vector fitting," *IEEE Trans. Power Del.*, vol. 14, no. 3, pp. 1052–1061, Jul. 1999.

[18] P. Yutthagowith and N. Pattanadech, "Improved least-square prony analysis technique for parameter evaluation of lightning impulsevoltage and current," *IEEE Trans. Power Del.*, vol. 31, no. 1, pp. 271–277, Feb. 2016.

[19] N. Pogaku, M. Prodanovic, and T. C. Green, "Modeling, analysis and testing of autonomous operation of an inverter-based microgrid," *IEEE Trans. Power Electron.*, vol. 22, no. 2, pp. 613–625, Mar. 2007.

[20] C. Dufour, H. Saad, J. Mahseredjian, and J. Bélanger, "Custom-coded models in the state space nodal solver of artemis," in *Proc. Int. Conf. Power Syst.Trans. (IPST-2013)*, 2013.